ELSEVIER

Structural evolution of PVDF during storage or annealing

M. Neidhöfer[a], F. Beaume[a,*], L. Ibos[b], A. Bernès[c], C. Lacabanne[c]

[a]Centre d'Etude de Recherche et Développement d'ATOFINA (CERDATO), Route du Rilsan, 27470 Serquigny, France
[b]Centre d'Etude et de Recherche en Thermique, Energétique et Systèmes (CERTES), IUT de Créteil, Université Paris XII Val de Marne,
61 avenue du Général de Gaulle, 94010 Créteil cedex, France
[c]Laboratoire de Physique des Polymères, L2P/CIRIMAT, Université Paul Sabatier, 118 route de Narbonne, 31062 Toulouse cedex, France

Abstract

The effect of annealing PVDF at temperatures above T_g and below T_m was investigated by differential scanning calorimetry (DSC), thermostimulated current spectroscopy (TSC) and solid-state NMR. This study evidences a progressive structural evolution, taking place during such annealing. Its characteristics (kinetics and its temperature dependence, lack of reversibility at lower temperature over extended periods of time, double organization corresponding to double annealing with unmodified kinetics) point to a mechanism of secondary crystallization as described by Marand et al. In addition to the formation of extra crystalline (hence rigid) material, this phenomenon is believed to generate increasing conformational constraints in the residual amorphous material. Accordingly, a progressive reduction of the molecular mobility was demonstrated by NMR during annealing.
© 2004 Elsevier Ltd. All rights reserved.

Keywords: Secondary crystallization; aging; annealing

1. Introduction

Secondary crystallization as a source of structural evolution has been extensively investigated by Marand and co-workers [1–4] on a variety of polymers including ethylene/octene copolymers, PEEK and polycarbonate. In their view, it corresponds to the progressive formation of a population of rather unstable crystals which melt at temperatures (noted T_m^{low}) slightly above their formation temperature and much lower than the melting temperature of primary crystals (noted T_m^{high}). Such secondary crystals are described as small clusters of organized neighboring chain segments forming bundle-like or fringed-micellar structures with virtually no or few reentry foldings. The chain segments involved in these structures likely originate from constrained amorphous regions in the vicinity of primary crystals, like cilia, tie chains and loose loops. By DSC, their melting results in a so-called low endotherm centered at T_m^{low}. This is opposed to the high endotherm centered at T_m^{high} which corresponds to melting of primary crystals, i.e. the usual lamellae structures which develop

from an unconstrained melt and include stabilizing reentry foldings that allow much larger dimensions for the crystals. The kinetics governing this secondary crystallization differs from those relative to primary crystallization. An important aspect of secondary crystallization is the progressive increase in conformational constraints within the residual amorphous fraction due to a crosslinking-like effect because of secondary crystals formation. One consequence of this conformational entropy reduction is the increase in melting point of the secondary crystals T_m^{low} with aging time. This approach is compared to Struik's formalism of physical aging in Ref. [4]. Recently, VanderHart and Snyder published evidences of structural evolution in isotactic polypropylene during aging at room temperature [5]. Their conclusions strongly support that 'the aging process can be viewed primarily as secondary crystallization rather than a generalized densification of the noncrystalline stems', but do not solve unambiguously the question of the morphological location of this secondary crystallization.

The purpose of the present paper is to bring evidence of the structural evolution in PVDF during storage/annealing over a wide range of temperature in between T_g and T_m and to examine how it fits with the secondary crystallization model of Marand et al.

* Corresponding author. Tel.: +33-232-466-730; fax: +33-232-466-889.
E-mail address: francois.beaume@atofina.com (F. Beaume).

2. Experimental

Two types of PVDF samples were used in this study. They differ mainly by their crystalline form and therefore are noted accordingly:

α-form PVDF samples were pellets of Kynar-720 manufactured by Atofina.

β-form PVDF samples were 40 μm thick Al-metalized and poled films provided by Solvay (Solef piezofilms).

2.1. DSC measurements

DSC experiments were performed with a TA Instruments 2920 Modulated DSC machine. Most experiments were run without modulation. Unless specified otherwise, the usual temperature range was from -40 to $200\,°C$ with heating and cooling rates equal to 20 K/min. A few experiments were performed with temperature modulation ($\pm 0.8\,°C$ every 60 s) superimposed on a 5 K/min heating rate. In this case, the temperature range spread from -20 to $140\,°C$. The temperatures measured on DSC traces were taken at the peak. The precise measurement of the enthalpy requires a more sophisticated processing [1–3] which was not undertaken in the present work. Therefore, only approximate values obtained directly from the DSC software without any correction are given as indications.

2.2. Pyroelectricity measurements (TSC)

Pyroelectricity measurements were carried out on a home-made thermostimulated current (TSC) spectrometer. All measurements were performed under dry Helium atmosphere in order to insure good thermal exchanges. The temperature of the sample cell is controlled with an accuracy of $\pm 1\,°C$. During experiments, aluminum metalized samples of poled β-form PVDF of area $S = 1\,cm^2$ were heated with a constant rate $\beta = 7\,°C/min$ from $-100\,°C$ up to $+90\,°C$. Samples were placed between two metallic electrodes short-circuited under a high sensitivity Keithley 642 ammeter in order to record the pyroelectric current I_T during heating runs. The current I_T is proportional to the pyroelectric coefficient p_3 of the material [6]:

$$I_T = p_3 S \beta \tag{1}$$

This pyroelectric coefficient is defined as the variation of the material polarization P above the variation of temperature T:

$$p_3 = \frac{dP}{dT} \tag{2}$$

The pyroelectric current measured is due to a reversible change of the polarization as a function of temperature: as the value of p_3 is always negative the macroscopic polarization P decreases when the temperature increases

[6,7]. As the value of the pyroelectric coefficient increases with temperature and S and β are kept constant during experiments the magnitude of the pyroelectric current I_T expresses the evolution of p_3 upon the temperature. Previous works have shown that the macroscopic polarization of β-form PVDF samples is stable only for temperatures below $+60\,°C$ [7,8]. If a temperature higher than $+60\,°C$ is reached, then an irreversible change in the polarization is observed [6–8]. This induces an attenuation of the value of the pyroelectric coefficient throughout the temperature range. In order to obtain a stable value of the pyroelectric coefficient during experiments and to obtain accurate and reproducible results, poled β-form PVDF samples were pre-conditioned prior to measurements. This was achieved by aging samples at $+90\,°C$ during 2 h 30 min inside the measurement device under short-circuited conditions. Indeed, it was previously demonstrated that this treatment allowed to obtain a stable pyroelectric activity for temperature values smaller than $+90\,°C$, i.e. the aging temperature [7]. Thus, subsequent annealing at a temperature of $+90\,°C$ or less should not reduce the macroscopic polarization.

2.3. NMR measurements

Broad-band NMR measurements were carried out on a Bruker MSL 300 spectrometer fitted with a standard Bruker ^{19}F static wideline probe. A roughly round pellet of the sample was centered in the 5 mm horizontal solenoid coil thanks to two glass spacers. The 90° pulse length was 3.0 μs. The ^{19}F free induction decays (FIDs) at 282.4 MHz were obtained using a simple single-pulse sequence, a recycling delay of 5 s, a dwell-time of 0.2 μs and acquisition of 4 K data points. They were then normalized to unity at the first data point. Owing to electronic dead time, this crude method prevents the observation of the very beginning of the FID. This may be a strong limitation for a quantitative interpretation. Nevertheless, our purpose here is more a qualitative comparison of FIDs. The FIDs were limited to eight accumulations only, allowing short enough experiments for a satisfying sampling of the aging kinetics, especially at the beginning.

3. Results and discussion

3.1. Evidence of the phenomenon

The DSC thermograms obtained on both α-form and β-form PVDF are shown in Fig. 1(a, b) and (c, d), respectively. The protocol is slightly different for both types of samples: α-form PVDF was heated from $-80\,°C$ up to $220\,°C$ in all three runs whereas β-PVDF was heated up to $100\,°C$ only in the first and second runs and then up to $220\,°C$ in the third run. The cooling rate here was -10 K/min. Such conditions allow to retain the β crystalline form in the β-form sample
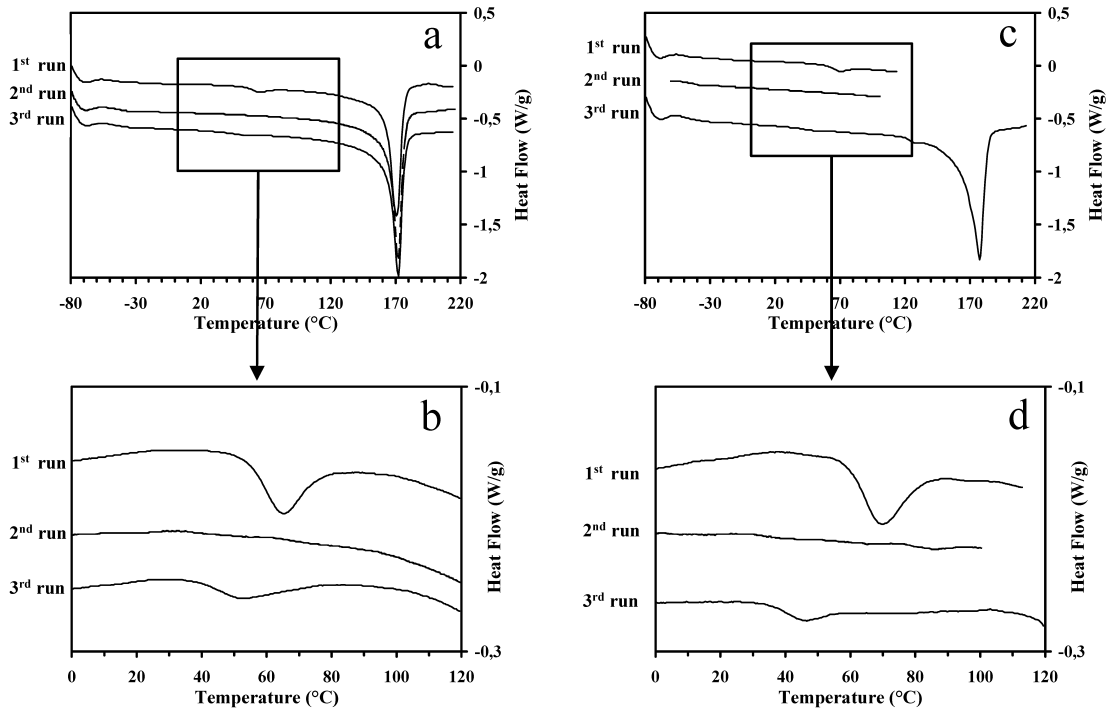
Fig. 1. DSC traces of (a,b) α-form PVDF and (c,d) β-form PVDF. The first run is immediately followed by the second run, whereas an annealing at room temperature for 5 h takes place before the third run (see text for details).

(until its melting in the third run), which would otherwise crystallize into the α modification if cooled from the melt. The α-form sample can be melted and then cooled without further precautions since PVDF crystallizes naturally into its α modification when cooled from the melt in the present conditions. For these reasons, melting is clearly visible on all three runs for α-form PVDF around 171 °C and on the third run only for β-form PVDF around 177 °C. The enthalpy was measured around 53.9 and 65.6 J/g for α-PVDF and β-PVDF, respectively, which corresponds to about 52 and 63% crystallinity assuming for both crystalline forms the same heat of fusion for 100% crystalline material (104.5 J/g) determined for α-PVDF [9].

On as-received samples, which have experienced storage at room temperature for months or perhaps even years, the first heating run reveals a small endothermic peak centered around 65 and 69 °C for α-form and β-form samples, respectively. This peak disappears in the second heating run performed immediately after cooling from the melt. But, when cooling from the melt is interrupted by an annealing at 23 °C for 5 h, the subsequent third heating run displays again this small endothermic peak but it appears now at a slightly lower temperature: 53 and 46 °C for α-form and β-form samples, respectively. Except for this temperature difference, both α-form and β-form PVDF exhibit the same behavior: the small peak is present with as-received samples, then disappears in the immediate second heating run, and then reappears after storage (or annealing) for a few hours at 23 °C. It will be called a DSC annealing-

peak hereafter. The enthalpy corresponding to this peak was estimated around 1.4 and 1.8 J/g in the first heating for α-PVDF and β-PVDF, respectively. These values amount to about 2.6–2.7% of the melting enthalpy around 170 °C mentioned above.

Using a similar protocol, β-form poled sample is characterized by TSC and the spectra are presented in Fig. 2. Again, the two first heating were limited to +90 °C to retain the β modification and to avoid a change in the pyroelectric activity. It is interesting to note that a small peak is clearly observed around 55 °C in the first heating run on the as-received sample (previously stored at room temperature for an unknown time), it then disappears in the immediate second heating run, and then reappears at a
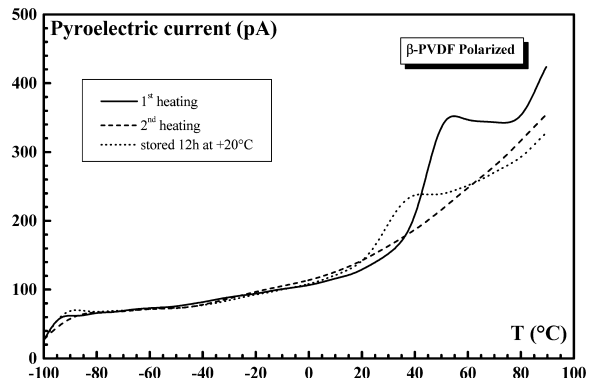

Fig. 2. Evolution of the pyroelectric current upon temperature for poled β-form PVDF (experimental conditions and annealing procedures are given in the text).

slightly lower temperature (about 40 °C) after annealing at room temperature for 12 h. It will be called a TSC annealing-peak by analogy with the DSC behavior.

Such DSC or TSC annealing-peaks have been reported already for PVDF and they were assigned to various origins: upper glass transition [10], reorganization within conformationally disordered α-crystals [11], molecular motions corresponding to an α_c relaxation in the crystalline/amorphous interface [12], melting of paracrystalline domains [13]. We must also stress that this phenomenon behaves so far in a very similar way as the low endotherm evidenced by Marand et al. on various other semi-crystalline polymers.

To get further insight, modulated DSC was used on an α-form sample in the third run of the experiment described above, i.e. after annealing at room temperature for 5 h. The corresponding MDSC traces are shown in Fig. 3. As evidenced already in Fig. 1, the total heat-flow (HF) exhibits a small annealing peak centered around 54 °C. More interesting is the evidence of this peak originating virtually exclusively from the non-reversible heat-flow contribution (NRHF). A very weak and broad reversible heat-flow contribution (RHF) cannot be totally excluded. This result tends to indicate that C_p change plays only a very minor role, if any. This conclusion appears in contradiction with previous assignments based on molecular motions only, such as T_g^{up} [10], or α_c relaxation in the crystalline/amorphous interface [12]. Nevertheless a small C_p jump accompanying a more intense endothermic phenomenon cannot be ruled out.

3.2. Kinetics

First melting and subsequent cooling result in a reproducible 'refreshed' state yielding no annealing-peak in an immediately following heating run. Starting from this reproducible state, the kinetics of the annealing-peak can be studied as a function of the annealing time prior to the heating run used for detection. The kinetics in α-form PVDF was investigated by DSC at three different annealing

temperatures, 23, 60 and 100 °C, and the corresponding traces are plotted in Fig. 4a–c, respectively. These annealings were performed in the DSC machine for annealing times up to 12 h. Longer annealing times at 23 °C correspond to storage at room temperature, which was close to 23 °C although the regulation is obviously not as good as in the DSC cell. At each temperature, a small annealing-peak already develops for an annealing time as short as 5 min (shorter times were not investigated) and is located about 10–15 °C above the annealing temperature. For longer annealing times, it shifts progressively towards higher temperatures and increases in size. This temperature evolution is plotted in Fig. 5. For each annealing temperature, the peak temperature shifts linearly with the log of annealing time and can be satisfactorily fitted with the
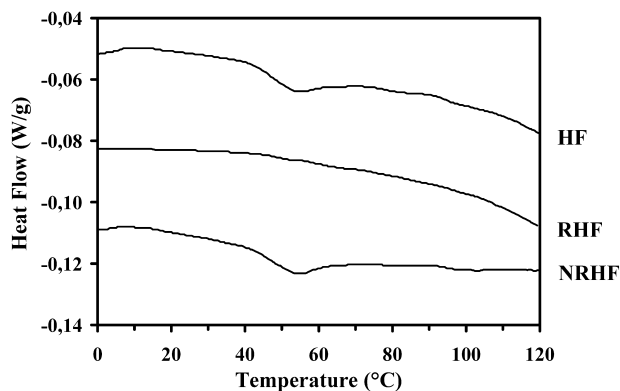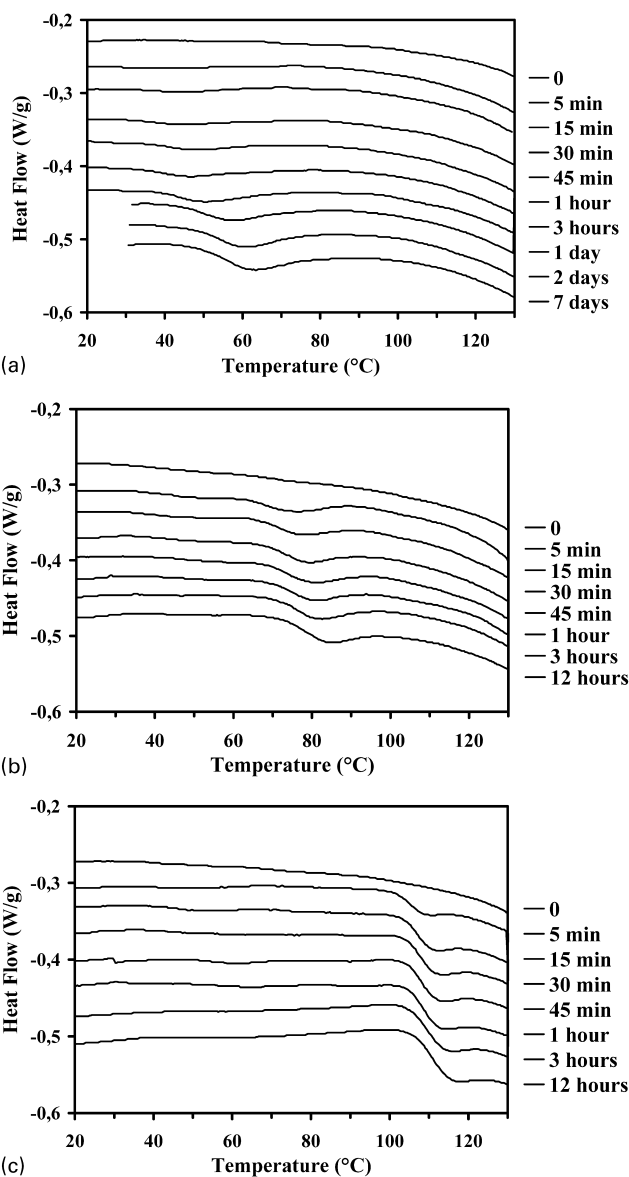

Fig. 3. MDSC traces of α-form PVDF after annealing at $T = 23$ °C for 5 h. The notations HF, RHF, NRHF refer to total heat-flow, reversible heat-flow and non-reversible heat-flow, respectively.

Fig. 4. DSC traces of α-form PVDF after annealing for various times at (a) $T = 23$ °C, (b) $T = 60$ °C, (c) $T = 100$ °C. The annealing time is indicated next to each trace.
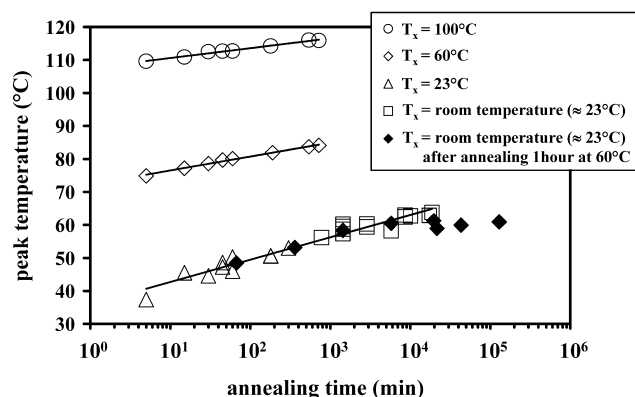
Fig. 5. Plot of the DSC annealing-peak temperature (T_m^{low}) as a function of annealing time (t_x) for α-form PVDF. For each annealing temperature T_x, the line corresponds to the best fit obtained with Eq. (3). The parameters resulting from the fit are given in Table 1.

equation proposed by Marand et al.:

$$T_m^{low} - T_x = A(T_x) + B(T_x)\ln(t_x) \qquad (3)$$

where T_m^{low} is the temperature of the annealing-peak and T_x and t_x are the annealing temperature and annealing time, respectively. The value obtained for the parameters $A(T_x)$ and $B(T_x)$ at each annealing temperature T_x are given in Table 1. It is interesting to note that the slope $B(T_x)$ decreases linearly with increasing temperature T_x and extrapolates to a null value for $T_{co} = 155$ °C. This behavior, opposite to a thermally activated process, is in agreement with the kinetic law ruling the secondary crystallization process described by Marand et al. for a variety of other semi-crystalline polymers. This strongly suggests that the annealing-peak is indeed a low endotherm corresponding to melting of PVDF secondary crystals formed during annealing.

In addition to T_m^{low}, Marand et al. have demonstrated that the enthalpy of the low endotherm ΔH_m^{low} conforms to a specific kinetic law, thus providing an additional specific feature which is another signature of the secondary crystallization. Such analysis requires a precise measurement of these rather small enthalpies, especially at short times, and was not performed in the present work. Nevertheless, estimates of the enthalpy were obtained using the conventional integration method available in the DSC software. These data exhibit an increasing trend, with values ranging
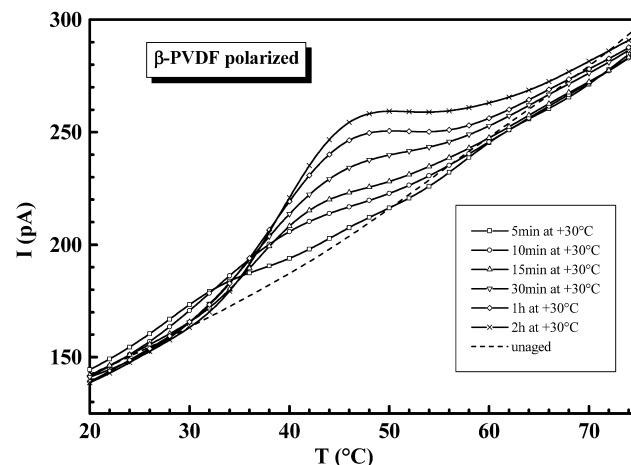

Fig. 6. Evolution of the TSC annealing-peak for poled β-form PVDF samples annealed for various times at +30 °C.

from about 0.2 to less than 2 J/g over the same time range as in Fig. 5. Such small values coupled with the limited accuracy of the present measurement and the lack of data at very short times prevent any further analysis of ΔH_m^{low} here.

The kinetics in β-form PVDF was investigated by TSC at a single annealing temperature, 30 °C, using samples 'refreshed' at 90 °C only to prevent a change in the macroscopic polarization. The corresponding traces are plotted in Fig. 6. Annealing treatments were performed inside the experimental device under short-circuited conditions. Moreover, pyroelectric samples are always short-circuited during cooling between consecutive runs. In a very similar way as the above mentioned DSC behavior of α-form PVDF, a small annealing-peak is already apparent after only 5 min annealing and it is centered at about 5 °C above the annealing temperature; it then develops and shifts towards higher temperatures with increasing annealing times. This temperature shift can be nicely fitted with Eq. (3) and the corresponding parameters are given in Table 1. The slope B observed by TSC on β-form PVDF at $T_x = 30$ °C appears in reasonable agreement with the corresponding slope observed by DSC on α-form PVDF at $T_x = 23$ °C. This result suggests that secondary crystallization develops independently of the predominant crystalline form of the primary crystals. A similar conclusion was proposed by Teyssedre et al. [12] although they assigned the phenomenon to a different origin. As Marand et al. proposed that

Table 1
Parameters describing the evolution of the annealing-peak temperature during annealing at various temperatures (Eq. (3))

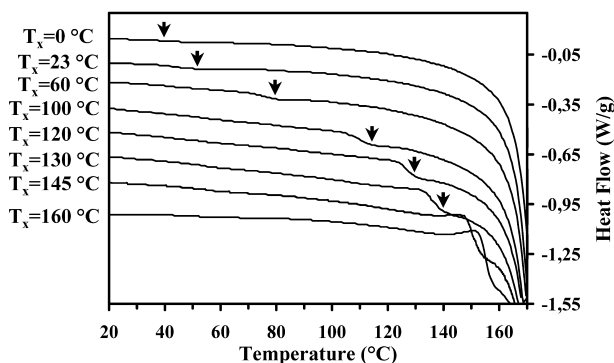| Technique	Sample	T_x (°C)	$A(T_x)$	$B(T_x)$
DSC	α-PVDF, refreshed at 200 °C	23	13.0	2.9
		60	12.3	1.8
		100	7.6	1.3
	α-PVDF, following preliminary annealing at 60 °C for 1 h (fit up to 6×10^3 min)	23	13.9	2.8
TSC	Poled β-PVDF, refreshed at +90 °C	30	5.0	3.1

Fig. 7. DSC traces of α-form PVDF after annealing for 3 h at various temperatures T_x. An arrow indicates the position of the endothermic peak in each case.

secondary crystallization involves topologically constrained chain segments, like loops and cilia and tie-chains, it seems not surprising that either α-form or β-form PVDF crystals could provide such environment. However, the presence of a significant α-form fraction in our predominantly β-form samples cannot be excluded.

3.3. Temperature range

So far, these results evidence an annealing-peak phenomenon over the temperature range 20–100 °C. As an extrapolated value as high as $T_{co} = 155$ °C was obtained from kinetics at various temperatures, the question is whether such a phenomenon can develop over an even wider range of temperature, and ultimately over the whole range between the glass transition ($T_g = -40$ °C) and melting ($T_m = 171–177$ °C). DSC and TSC experiments were conducted over a wide range of annealing temperature on α-form (0; +160 °C with 3 h annealing time) and β-form (−10; +40 °C with 1 h annealing time) PVDF, respectively. The results are plotted in Figs. 7 and 8, respectively. For annealing above room temperature, DSC traces on α-
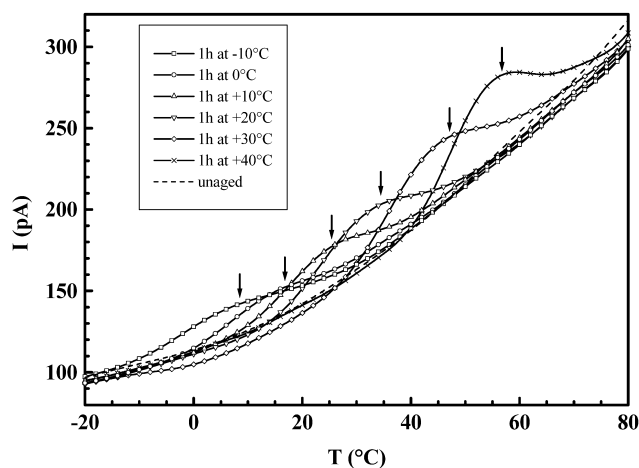
form PVDF exhibit an annealing-peak which shifts according to annealing temperature up to an annealing temperature of 130 °C. With a constant annealing time $t_x = 3$ h, the observed temperature difference $\Delta T = T_m^{low} - T_x$ is progressively reduced with increasing annealing temperature T_x, as expected from Eq. (3) and the temperature dependence of both $A(T_x)$ and $B(T_x)$ parameters (see Table 1). Higher annealing temperatures (145 and 160 °C) result in a shoulder on the low temperature side of the melting endotherm as if the annealing-peak had merged into the melting peak. In addition, a broad endotherm below the annealing temperature is visible prior to the shoulder. Therefore, it is likely that annealing at such temperatures close to or even within the melting zone modifies the primary crystalline structure and perhaps even the crystalline form [14]. β-form PVDF probed by TSC over a narrower range of annealing temperature exhibits essentially the same behavior as α-form PVDF (probed by DSC) within the same temperature range. For annealing below room temperature, a single DSC experiment was performed with α-form PVDF at 0 °C and results in a hardly visible annealing-peak. Fortunately, TSC experiments on β-form PVDF yield a much higher sensitivity (although the annealing time is shorter) and clearly confirm that the annealing-peak phenomenon is still efficient at least down to −10 °C and behaves just like above room temperature. These results indicate that the annealing-peak phenomenon can develop over most of the temperature range between glass transition and melting.

3.4. Reversibility and double annealing

As the temperature position of the annealing-peak reflects the annealing temperature, it could provide a signature of the storage temperature or the usage temperature as long as this phenomenon is not reversible. In order to check this point, double annealing experiments were conducted. Fig. 9 presents the DSC traces obtained on α-form PVDF after a first annealing at 60 °C for 1 h followed

Fig. 8. Evolution of the TSC annealing-peak for poled β-form PVDF samples annealed for 1 h at various temperatures.

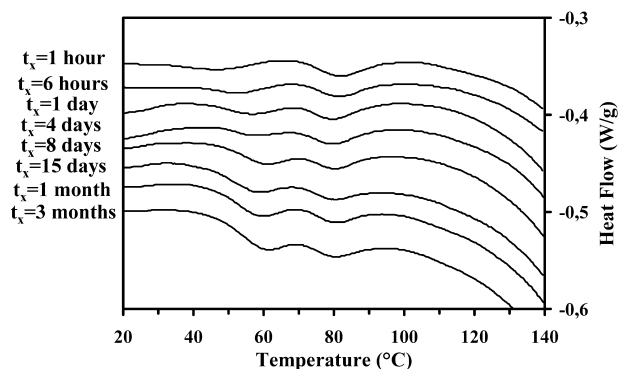
Fig. 9. DSC traces of α-form PVDF after a double annealing. The first annealing at +60 °C for 1 h is the same for all different traces. Then the second annealing takes place at room temperature for various times t_x as indicated next to each trace.

by a second annealing at room temperature (regulated around 23 °C) for various times. The expected annealing-peak corresponding to the first annealing is observed around 80 °C, in agreement with results in Figs. 4b and 5, whatever the subsequent annealing time at room temperature. In addition a second annealing-peak appears around 55 °C after 1 h (no shorter times were investigated) and shifts progressively towards higher temperatures as the second annealing time is increased. This behavior of the second annealing-peak is in good agreement with results above for a single annealing in similar conditions. Furthermore, the kinetics of the annealing-peak developing during storage at room temperature after a preliminary annealing at 60 °C is compared in Fig. 5 to its equivalent developing from the 'refreshed' state described before. The peak temperature T_m^{low} conforms to an identical log dependence upon annealing time up to about 10^4 min (see Fig. 5 and parameters from the fit in Table 1). This is in agreement with Marand's experiments on PEEK [2] which showed that the kinetics for an annealing at $T_x = 210$ °C was identical with or without preliminary annealing at higher temperature (300 °C for 1 h).

For longer annealing times, the evolution of T_m^{low} in the double annealing experiment appears to level off and reach a plateau or reduced slope regime. Unfortunately, such long annealing times were not explored and no plateau regime was observed in the single annealing experiments. Nevertheless, VanderHart and Snyder proposed a slowing down kinetics at long annealing times as a possible reason for a data point at more than 10^6 min aging time falling below the extrapolation based on data up to 5×10^3 min aging time [5].

During the build-up of this second annealing-peak, the first annealing-peak does not appear to decrease in intensity or shift significantly, even for times as long as three months, although the partial overlapping of both endotherms makes a precise quantitative analysis difficult. Similar observations were reported for PEEK [2] although the second annealing time was kept much 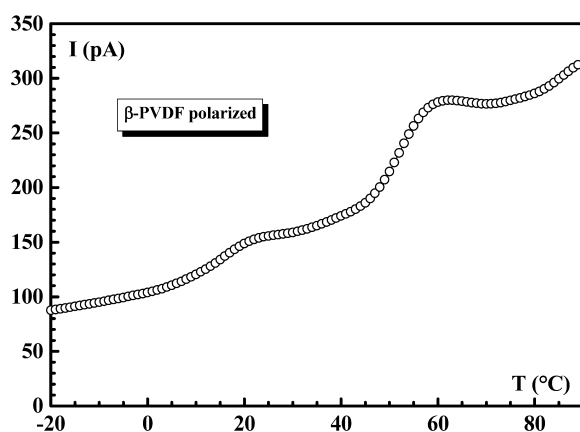shorter. Therefore these results tend to indicate that the annealing-peak phenomenon is not reversible at a lower temperature. Of course, if the double annealing is inverted (i.e. annealing at lower temperature first and at higher temperature afterwards) what has developed during the first annealing is destroyed during the second one, resulting in a single annealing-peak only which corresponds to the second annealing (not shown).

Presented in Fig. 10, a TSC experiment of double annealing on β-form PVDF confirms a similar behavior as described above for DSC measurements on α-form PVDF: a high temperature annealing-peak (around 60 °C) corresponding to the first high temperature annealing (at 40 °C for 2 h) and an additional low temperature annealing-peak (around 20 °C) corresponding to the subsequent low temperature annealing (at 0 °C for 2 h). Again, this secondary crystallization phenomenon appears rather independent of the predominant crystalline form α or β.

3.5. Influence of the macroscopic polarization magnitude

The TSC annealing-peak can be interpreted as a depolarization peak occurring during the heating procedure. This induces that the material polarization should be increased significantly during storage at room temperature [6,7]. Thus, the reorganization of polymeric chains during storage seems to go with a preferential orientation of dipoles that increases the macroscopic polarization of the material. In order to investigate the influence of the material polarization on the TSC annealing peak, poled β-form PVDF samples aged for 2 h 30 min at temperatures ranging from +70 to +150 °C were investigated. These aging procedures carried out prior to pyroelectric measurements allowed to obtain different stable values of the material macroscopic polarization. After this aging procedure, aged samples were kept at room temperature for 12 h. Then, two consecutive pyroelectric measurement runs were performed for each sample investigated. By subtracting the two consecutive pyroelectric current recorded, it was possible
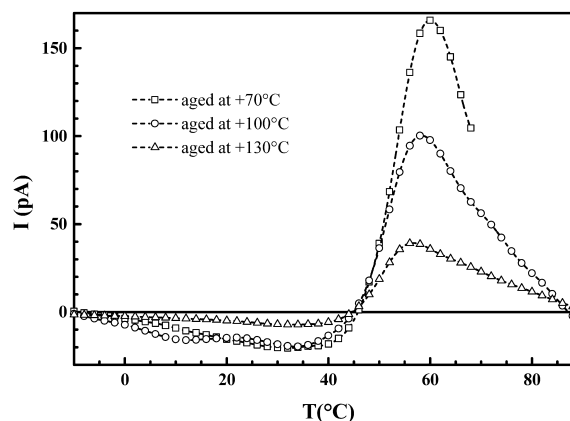
Fig. 10. 'Double' TSC annealing-peak observed on a poled β-form PVDF sample annealed successively for 2 h at +40 °C and 2 h at 0 °C.

Fig. 11. TSC annealing-peak obtained for poled β-form PVDF samples aged at various temperatures (+70, +100 and +130 °C) and then stored for 12 h at room temperature. The plots were obtained by subtracting two consecutive pyrocurrent spectra.
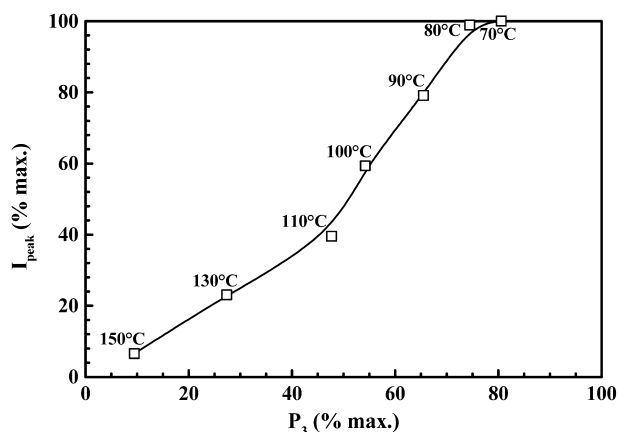
Fig. 12. Evolution of the TSC annealing-peak normalized magnitude of poled β-form PVDF samples upon the normalized value of the pyroelectric coefficient at room temperature (see text for details).

to isolate the TSC annealing peaks signature [8]. Three TSC annealing-peaks obtained for samples aged at $+70$, $+100$ and $+130\,°C$, respectively, are presented on Fig. 11. The amplitude of this peak decreases when increasing the aging temperature, i.e. when the material polarization is reduced. Fig. 12 summarizes the results obtained for all aged sample investigated. In this figure, the TSC annealing-peak normalized magnitude (referenced to the $+70\,°C$ aged sample) is plotted upon the normalized value of the pyroelectric coefficient at room temperature. This normalized value of p_3 was calculated as the ratio between the value of the pyroelectric coefficient at room temperature for a non-aged sample and its value at the same temperature after the aging treatment. In fact, the value of the pyroelectric coefficient reflects here the magnitude of the macroscopic material polarization. So, we can observe here that the magnitude of the TSC annealing-peak decreases gradually as the material polarization vanishes. This result confirms that a reorientation of dipoles occurs in poled β-form PVDF during chains reorganization and that this preferential dipole orientation is
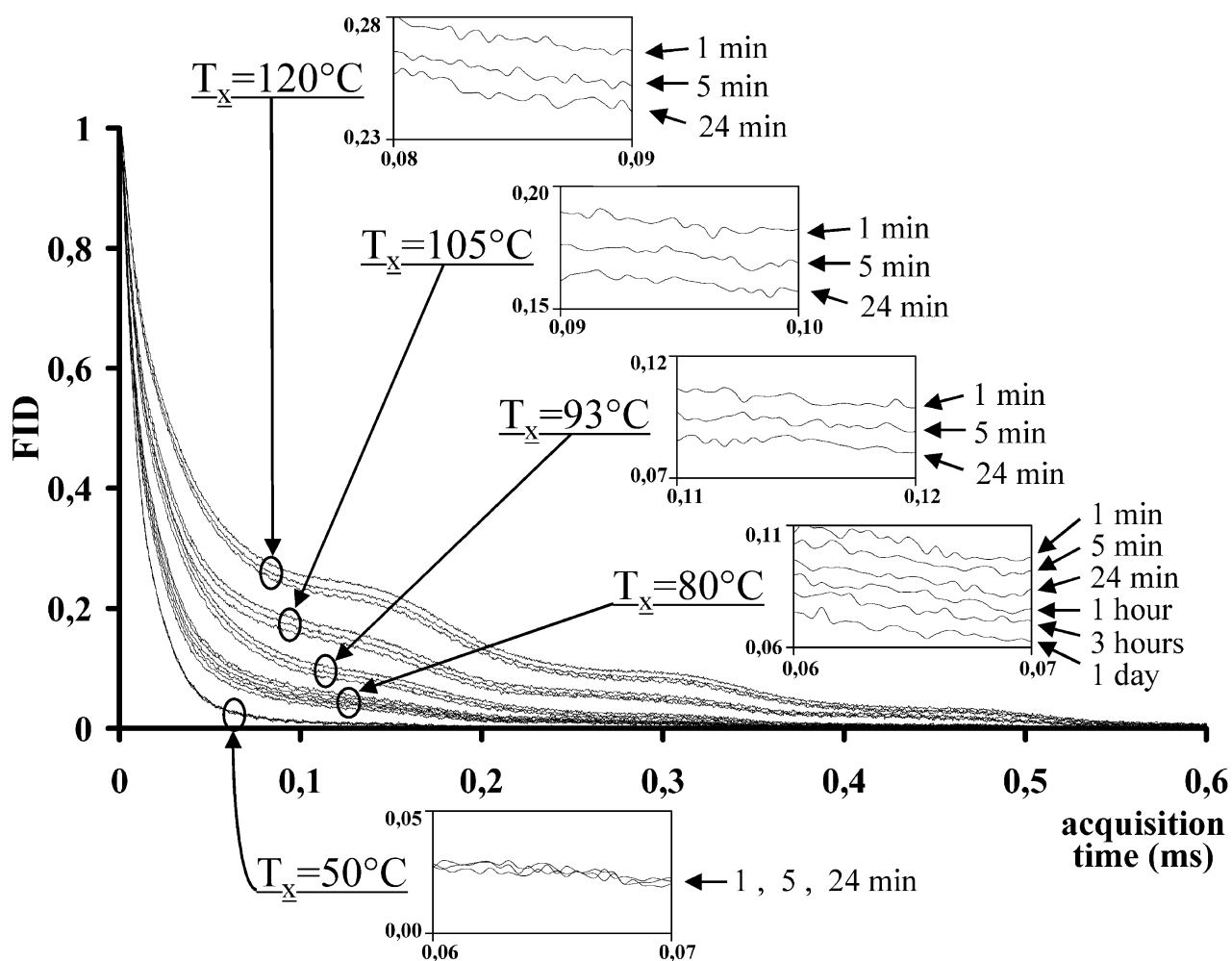

Fig. 13. Broad-Band ^{19}F NMR: FIDs are recorded after various annealing time (t_x) at the same temperature as the annealing temperature (T_x), as indicated in the figure. The inserts present the same data with a $\times 4$ magnification. It appears clearly that during annealing at $T_x = 120, 105, 93$ and $80\,°C$, the mobility is progressively reduced.

directly depending on the macroscopic polarization. Moreover, this preferential dipole orientation seems to be induced by the local electric field created by crystallites. Finally, these ultimate results demonstrate unambiguously that the TSC annealing-peak originates from the disorientation of organized domains formed during annealing or storage.

3.6. Molecular mobility during annealing

All information presented so far consists in indirect evidences of the structural evolution: the so-called annealing-peaks correspond to destruction/melting of organized domains which have formed during storage/annealing. In order to gain direct evidences of the phenomenon, solid-state NMR experiments were conducted on α-form PVDF. They consist in ^{19}F single-pulse experiments which are less than 1 min long and therefore enable a reasonable sampling of the phenomenon (NMR measurements are taken without varying the temperature during the annealing, which is conducted directly in the NMR probe). Prior to this monitoring of the annealing, the sample was heated up to 140 °C for 10 min and then cooled down to the annealing temperature within the NMR probe to ensure a 'refreshed' state as starting point of the annealing. The results obtained at five different annealing temperatures are presented in Fig. 13.

For each annealing temperature T_x, a series of FIDs is obtained corresponding to various annealing times t_x as indicated in Fig. 13. Comparing FIDs obtained after the same $t_x = 1$ min (i.e. with virtually no annealing), an obvious evolution is associated with temperature. At $T_x = 50$ °C, the FID is largely dominated by rigid contributions corresponding to fast decaying signals. When T_x is increased, more mobile contributions appear as slower decaying signals that eventually become modulated at $T_x = 93$ °C and above, as several resonances become resolved as expected from the high-resolution ^{19}F spectrum of PVDF [15]. In the present experiment, 'rigid' and 'mobile' refer to dynamics of the order of 10^5 Hz which are most efficient in averaging dipolar couplings.

More interesting is the evolution of FIDs observed within each series in Fig. 13: for all annealing temperatures except the lowest one ($T_x = 50$ °C), the signal decay appears continuously accelerated as annealing proceeds. This trend clearly reflects a progressive reduction of the molecular mobility during annealing. It is to be reminded that the magnitude of the FIDs evolution does not provide a direct quantitative measurement of the reduction in mobility as the various dynamical modes contribute with different efficiencies to the averaging of dipolar interactions (the most efficient being of the order of 10^5 Hz). The ultimate situation corresponds to annealing at the lowest temperature investigated here, $T_x = 50$ °C, where the population of highly efficient dynamical modes is already very limited in the refreshed state (dynamics probably too slow) and

therefore a further reduction does not significantly affect the FID.

These experiments provide a direct evidence of a reduction in molecular mobility during annealing. This result is in agreement with the model proposed by Marand et al. (formation of secondary crystals inducing conformational constraints in the residual amorphous) and further supports the existence of such a structural evolution in PVDF during storage or annealing above T_g.

4. Conclusion

PVDF undergoes a structural evolution during annealing over a wide range of temperature between T_g and T_m. The organization that develops during such annealing can be destroyed at a slightly higher temperature, yielding a small endotherm on the DSC trace centered at T_m^{low}. The kinetics of the phenomenon, as seen through the T_m^{low} value, exhibits a log dependence versus annealing time. Its slope, $B(T_x)$, decreases with increasing annealing temperature T_x, indicating a surprisingly slower kinetics at higher temperature. No indication of reversibility at lower temperature was obtained over times as extended as 3 months. When first annealing is followed by a second annealing at a lower temperature (double annealing), a double endotherm is observed. The kinetics of the second one appears not to be affected by the first one. All these results for PVDF are in agreement with the structural evolution and its characteristics described by Marand et al. in several other polymers and which is assigned to secondary crystallization accompanied by increasing conformational constraints in the residual amorphous material. No influence of the predominant crystalline form α or β was observed in the present work. In β-form PVDF samples, a preferential orientation of dipoles superimposed to the structural evolution yielding to an increase of the macroscopic polarization was evidenced. In addition to the indirect evidences mentioned above, solid-state NMR experiments have brought direct evidences of a progressive reduction in molecular mobility during the annealing itself.

References

[1] Alizadeh A, Richardson L, Xu J, McCartney S, Marand H, Cheung YW, Chum S. Macromolecules 1999;32:6221–35.
[2] Marand H, Alizadeh A, Farmer R, Desai R, Velikov V. Macromolecules 2000;33:3392–403.

[3] Alizadeh A, Sohn S, Quinn J, Marand H, Shank LC, Darrell Iler H. Macromolecules 2001;34:4066–78.

[4] Marand H, Alizadeh A, Sohn S, Xu J, Farmer R, Prabhu V, Cronin S, Velikov V. ANTEC 2001;2:1856–9.

[5] VanderHart DL, Snyder CR. Macromolecules 2003;36:4813–26.

[6] Teyssèdre G. Transitions et relaxations diélectriques dans les copolymères ferroélectriques poly(fluorure de vinylidène/trifluor-oéthylène), Thesis, University Toulouse III, France; 1993.

[7] Ibos L, Teyssèdre G, Bernès A, Lacabanne C. Polymers and liquid crystals. Proc SPIE 1999;4017:29–36.

[8] Kolbeck AG. J Polym Sci: Phys Ed 1982;20:1987–2001.

[9] Nakagawa K, Ishida Y. J Polym Sci: Polym Phys Ed 1973;11: 2153–71.

[10] Leonard C, Halary JL, Monnerie L, Micheron F. Polym Bull 1984;11: 195–202.

[11] Loufakis K, Wunderlich B. Macromolecules 1987;20:2474–8.

[12] Teyssèdre G, Bernès A, Lacabanne C. J Polym Sci: Part B: Polym Phys 1993;31:2027–34.

[13] Nabata Y. Jpn J Appl Phys 1990;29(12):2782–8.

[14] Lovinger AJ. In: Basset DC, editor. Developments in crystalline polymers, vol. 1. London: Applied Science Publishers; 1981.

[15] Wormald P, Apperley DC, Beaume F, Harris RK. Polymer 2003;44: 643–51.